

# Scalar field dark matter: helping or hurting small-scale problems in cosmology?

Victor H. Robles, <sup>1★</sup> James S. Bullock <sup>1</sup> and Michael Boylan-Kolchin <sup>©2</sup>

<sup>1</sup>Department of Physics and Astronomy, University of California, Irvine, 4129 Frederick Reines Hall, Irvine, CA 92697, USA

Accepted 2018 November 20. Received 2018 October 22; in original form 2018 July 19

#### ABSTRACT

Building upon results of cosmological simulations of ultra-light scalar field dark matter (SFDM), we present a comprehensive model for the density profiles of SFDM haloes as a function of halo virial mass  $M_h$  and scalar field mass m. The central regions of SFDM haloes are dominated by solitons with characteristic densities that increase with increasing halo mass and asymptote to CDM-like profiles at large radii. For scalar field masses  $m\sim$  $10^{-22}$  eV, consistent with large-scale structure observations,  $M_h \sim 10^{10} \,\mathrm{M_\odot}$  haloes have lower core densities than their cold dark matter (CDM) counterparts and this alleviates the too big to fail problem in a regime where feedback is less effective. However, higher mass SFDM haloes with  $M_h \sim 10^{11} \, \mathrm{M}_\odot$  are denser than their CDM counterparts at small, observationally relevant radii. We use rotation curves of  $V \sim 100 \, \mathrm{km \ s^{-1}}$  galaxies from the SPARC database to show that SFDM exacerbates the cusp/core and central density problems seen in CDM at this scale. We conclude that if the conventional cosmological SFDM scaling relations are correct, then baryonic feedback is required to lower densities in SFDM haloes even more so than in CDM. This motivates cosmological and self-consistent hydrodynamic simulations of SFDM to determine whether central soliton structure can be altered by realistic feedback implementations.

**Key words:** methods: numerical – galaxies: haloes – dark matter.

#### 1 INTRODUCTION

The nature of dark matter is one of the greatest puzzles in astrophysics and cosmology. The standard cold dark matter (CDM) model assumes that most of the matter content of the Universe is in the form of a non-interacting and non-relativistic matter component. Under these assumptions, the model has successfully described large-scale cosmological observations (Vogelsberger et al. 2014; Planck Collaboration XXIII 2015; Guo et al. 2016), but it has mismatches with observations at much smaller scales (Bullock & Boylan-Kolchin 2017). Well-known issues include the cusp/core and central density problems inferred from inner rotation curve shapes (Flores & Primack 1994; Moore 1994; Karukes, Salucci & Gentile 2015), the too big to fail (TBTF) problem associated with lower-than-expected central densities of small dwarf galaxies (Boylan-Kolchin, Bullock & Kaplinghat 2011), and the missing low-mass galaxy problem (Klypin et al. 1999; Moore et al. 1999).

It is possible that a better understanding of baryonic processes will resolve these issues. Supernova feedback, for example, can reduce the dark matter density in the cores of galaxies (Navarro, Eke & Frenk 1996; Governato et al. 2012; Brooks et al. 2013; Chan et al. 2015; Oñorbe et al. 2015; Read, Agertz & Collins 2016), but only if the galaxy produces enough stars (Peñarrubia et al. 2012; Garrison-Kimmel et al. 2013; Di Cintio et al. 2014; Oñorbe et al. 2015; Fitts et al. 2017). Stellar feedback in many simulations can only efficiently remove dark matter from within a galaxy's half-light radius (Fitts et al. 2017). Therefore, dark matter density discrepancies in the smallest dwarf galaxies and at large radii are more difficult to explain with baryonic feedback (Papastergis et al. 2015; Bullock & Boylan-Kolchin 2017).

Alternatively, the small-scale issues may point to something deeper about the nature of dark matter. For example, if the dark matter particles have strong self-interactions (Spergel & Steinhardt 2000; Kaplinghat, Tulin & Yu 2016), the resulting flattening of density cusps into cores can alleviate central density problems (Vogelsberger, Zavala & Loeb 2012; Rocha et al. 2013; Zavala, Vogelsberger & Walker 2013; Elbert et al. 2015; Vogelsberger et al. 2016; Robles et al. 2017). If the dark matter is a thermal relic of appropriate mass ( $m \sim \text{keV}$ ), it behaves as warm dark matter (WDM), streaming freely in the early Universe to suppress small-scale power. This completely prevents the formation of small dark matter haloes and makes dwarf-size dark matter haloes form later and with lower overall densities compared to CDM (Bond, Szalay & Turner 1982;

<sup>&</sup>lt;sup>2</sup>Department of Astronomy, The University of Texas at Austin, 2515 Speedway, Stop C1400, Austin, TX 78712-1205, USA

<sup>\*</sup> E-mail: vrobles@fis.cinvestav.mx

Bode, Ostriker & Turok 2001; Schneider et al. 2012; González-Samaniego, Avila-Reese & Colín 2016; Bozek et al. 2016; Horiuchi et al. 2016).

This work focuses on another possibility: that the dark matter is an ultralight ( $m \sim 10^{-22}$  eV) scalar field with negligible selfinteractions (Lee & Koh 1996; Hu, Barkana & Gruzinov 2000; Matos, Guzmán & Ureña-López 2000; Amendola & Barbieri 2006; Lundgren et al. 2010; Hui et al. 2017; Suárez & Chavanis 2017). At early times, the field oscillates like a classical axion and has energy density that redshifts like matter ( $\rho \propto a^{-3}$ ). On large scales, the model mirrors CDM. On small scales, however, the phenomenology is quite different. The ultralight mass gives a de Broglie wavelength that is astrophysically significant ( $\lambda_{dB} \sim 0.1-1$  kpc). This produces an effective quantum pressure that suppresses power below a Jeans scale and prevents the formation of very small haloes ( $M_{
m min}$   $\sim$  $10^8 \text{ M}_{\odot}$ ). For the larger haloes that do form, the quantum pressure prevents the formation of a central cusp that is characteristic of CDM and WDM haloes. Galaxy haloes composed of ultralight scalars have density profiles that are distinctive, with a central 'soliton' embedded within a familiar CDM-like outer halo (Matos & Ureña-López 2004; Böhmer & Harko 2007; Sikivie & Yang 2009; Suárez & Matos 2011; Chavanis 2012; Robles & Matos 2012, 2013; Li, Rindler-Daller & Shapiro 2014; Marsh & Silk 2014; Bernal, Robles & Matos 2017). Though dark matter of this class has been explored extensively for almost two decades, it has somewhat confusingly been referred to by many different names. Frequent terms include Bose-Einstein condensate dark matter, ultralight dark matter, WDM,  $\psi$ DM, and fuzzy dark matter. We adopt 'scalar field dark matter' (SFDM) here because a literature search showed this name to be the most common.

Current constraints on SFDM from structure formation and CMB data provide lower bounds on the scalar field mass (Matos, Vázquez-González & Magaña 2009; Bozek et al. 2015; Hlozek et al. 2015; Sarkar et al. 2016). For example, Amendola & Barbieri (2006) used Lyman  $\alpha$  forest constraints to limit  $m > 0.5 \times 10^{-22}$  eV. Bozek et al. (2015) and Schive et al. (2016) both find  $m \gtrsim 1 \times 10^{-22}$  eV from reionization and high-redshift UV-luminosity function comparisons. We adopt  $m > 0.8 \times 10^{-22}$  eV as a conservative lower limit on the scalar field mass in what follows.

Galaxy rotation curves and kinematic data for dwarf galaxies in the Local Group suggest that scalar field masses in the range  $m \simeq 0.1-5 \times 10^{-22} \, \text{eV}$  provide better agreement on dwarf-galaxy scales than CDM. Specifically, this mass range produces constantdensity soliton cores of size ~0.1-1 kpc in dwarf galaxies (Lora et al. 2012; Lora & Magaña 2014; Lora 2015; Martinez-Medina, Robles & Matos 2015; Robles et al. 2015; Calabrese & Spergel 2016; Chen, Schive & Chiueh 2017; Ureña López, Robles & Matos 2017). Taken together with the lower limits provided by structure formation, these efforts pinpoint a mass range  $m \simeq 0.8$ - $5 \times 10^{-22}$  as astrophysically interesting for SFDM. While substantially higher values of m are likely to be consistent with available structure formation and galaxy-scale constraints, such models do not result in observationally relevant dark matter cores (in the absence of baryonic physics), so we do not consider such models here.

Several authors have provided analytic self-gravitating solutions for SFDM haloes in spherically symmetric configurations (Gleiser 1988; Seidel & Suen 1994; Balakrishna, Seidel & Suen 1998; Ureña López 2002; Guzmán & Ureña López 2004, 2006). It is now well established that SFDM admits stable, minimum-energy configurations that are attractor solutions in the presence of small perturbations. These stationary solutions are referred as 'solitons' (Gleiser &

Watkins 1989; Lee 1989; Seidel & Suen 1990, 1994; Guzmán & Ureña López 2004; Chayanis 2011, 2016).

Only recently has it been possible to conduct a fully self-consistent SFDM simulation within a cosmological volume (Schive, Chiueh & Broadhurst 2014). These DM-only SFDM simulations confirmed the existence of a compact and stable self-gravitating soliton at the centres of SFDM haloes. Further, these authors found that the central soliton is surrounded by a turbulent medium dominated by less dense fluctuations with characteristic sizes similar to that of the soliton. Though these simulations represent a major achievement, the demanding constraints on spatial resolution have demanded fairly small comoving volumes, and thus an exploration of the statistical halo properties was not feasible.

Non-cosmological (idealized) simulations are much less computationally expensive to run and this approach has provided a useful avenue for insight into the process of relaxation and halo collapse in SFDM. Schwabe, Niemeyer & Engels (2016), for instance, studied two-soliton merger interactions for different halo parameters. Similarly, Mocz et al. (2017) conducted simulations of multiple soliton cores merging, characterizing properties of the central dense soliton and the outer turbulent density field. These studies have provided results consistent with those of Schive et al. (2014) and showed that the SFDM halo profile beyond the core soliton resembles a Navarro, Frenk & White (1997, hereafter NFW) profile as seen in CDM simulations. Mocz et al. (2017) showed that in this outer NFW-like region, SFDM halo structure is governed by an equipartition between potential, classical kinetic, and quantum gradient energies, whereas the quantum gradient energy supports the profile inside the soliton.

Mocz et al. (2017) also found that there is a dominant mode (wavelength) that contains most of the energy in the turbulent medium. Interestingly, this characteristic wavelength that seeds most of the interference sets a preferential length scale, which is observed to be about the soliton diameter. The existence of a preferential scale for interference leads to the possibility that the average density field will not be completely smooth, but have small amplitude oscillations resulting from the net effect, the degree of smoothness is related to the size of the soliton, which itself is modified by the total mass distribution. In this work, we will not consider the modelling of the fluctuating field.

In what follows, we provide a comprehensive method for predicting the density profiles of non-self-interacting SFDM haloes as a function of halo virial mass. The resultant density profiles capture the expected mass distributions of a broad range of SFDM haloes and can be used to compare to observations. Building on the results of cosmological simulations in both SFDM and CDM, our procedure matches the inner soliton prediction to the outer NFW-like profile at large radius.

In Section 2, we summarize the current understanding of inner soliton structure as a function of halo virial mass, present our formalism to connect the soliton region to the outer CDM-like profiles, and discuss the expected scatter in outer dark matter mass distributions for a given halo mass using our model. In Section 3, we use our results to confront the TBTF problem for low-mass dwarf galaxies as well as the rotation curve shapes of higher mass galaxies and show that a single scalar field mass has difficulty resolving both problems simultaneously. Our results set a first step to model haloes that are currently beyond the SFDM simulation capabilities, motivating further progress in large-scale cosmological BEC/SFDM simulations to better constrain the scatter we predict in dark matter density profiles for a fixed halo mass and SFDM particle mass *m*.

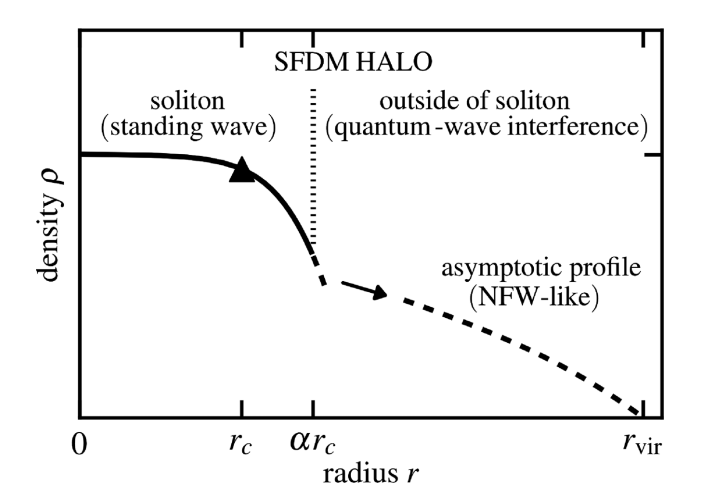


Figure 1. Schematic diagram of the density profile of a SFDM halo. The central region is dominated by a soliton of characteristic radius  $r_c$  set by the halo virial mass  $M_h$  and scalar field mass m:  $r_c \sim \lambda_{\rm dB} \propto m^{-1} \, M_h^{-1/3}$ . The outer region asymptotes to a CDM-like NFW profile. The transition from the soliton to the outer halo occurs at a radius  $r = \alpha \, r_c \sim 3 \, r_c$  (vertical dotted line) and is marked by an abrupt change in average density profile slope. In this region, the dark matter is mildly turbulent with density fluctuations of characteristic physical size  $\sim \lambda_{\rm dB}$ .

# 2 SFDM DENSITY PROFILES

Fig. 1 shows a schematic representation of our current understanding of the expected structure of an SFDM halo with virial radius  $r_{\rm vir}$ . The structure is characterized by an inner soliton of radius  $r_c \sim \lambda_{\rm dB}$  and an outer profile that asymptotes to the expectation for CDM haloes at large r. The soliton is embedded within a turbulent medium, and envelope of dark matter that asymptotes to the CDM solution as  $r \rightarrow r_{\rm vir}$ . The transition from the soliton core to the outer halo occurs at a radius  $r = \alpha r_c$ , where  $\alpha \sim 3$  (vertical dotted line) and is usually marked by a discontinuous slope.

Below, we provide a self-consistent parametrization of the full density profile of SFDM haloes and use it to estimate the expected scatter in the dark matter mass distribution beyond the soliton radius. In our approach, we join the inner soliton to the outer region at  $r=\alpha\,r_c$  and explore a range of  $\alpha$  values informed by numerical simulations and physically motivated limits. Our values range from  $\alpha\sim 2$  for dwarf-size haloes to  $\alpha\sim 3-4$  for Milky Way size haloes. We start by summarizing what is known about soliton cores and their structure as a function of halo mass.

# 2.1 Soliton cores

The structure of an SFDM halo is governed by the Schrodinger–Poisson (SP) equations for a self-gravitating scalar field with associated gravitational potential *V*:

$$i\hbar \frac{\partial \psi}{\partial t} = -\frac{\hbar^2}{2m} \nabla^2 \psi + mV\psi$$

$$\nabla^2 V = 4\pi G(\rho - \overline{\rho}), \tag{1}$$

where  $\psi$  is the wavefunction and  $\rho = |\psi|^2$  is the DM density (see e.g. Chavanis 2011).

Using cosmological simulations, Schive et al. (2014) found that all collapsed haloes develop a central soliton core described by the ground state solution of the SP equations. They found that the

central core region was well fit by the profile

$$\rho_{\text{sol}}(r) = \frac{\rho_c}{\left(1 + 0.091 \left(\frac{r}{r_c}\right)^2\right)^8},\tag{2}$$

where  $\rho_c$  is the central density given by

$$\rho_c = 1.93 \times 10^7 \, m_{22}^{-2} \left( \frac{r_{\rm c}}{1 \, \rm kpc} \right)^{-4} \, \rm M_{\odot} kpc^{-3}, \tag{3}$$

with

$$m_{22} \equiv \frac{m}{10^{-22} \,\text{eV}/c^2}.\tag{4}$$

Note that for fixed m, the soliton density scales inversely with soliton size such that the smallest solitons are physically denser:  $\rho_c \propto m^{-2} r_c^{-4}$ . These scalings between density, radius, and scalar field mass are demanded by the symmetry of the SP equations (Schive et al. 2014).

The soliton structure is governed by the global potential envelope of the halo it inhabits. We expect its size to be similar to the de Broglie wavelength  $r_c \sim \lambda_{\rm dB} \equiv h/(m\,v)$ . In a collapsed halo of virial mass  $M_{\rm h}$ , the characteristic velocity increases with halo mass as  $v \propto M_{\rm h}^{1/3}$ , which implies  $r_c \propto m^{-1} M_{\rm h}^{-1/3}$ . Schive et al. (2014) used the cosmological simulations of Schive et al. (2014) to obtain a relation between the soliton core and its host halo; at z=0, they found

$$r_c = 1.6 \,\mathrm{kpc} \left(\frac{M_{\rm h}}{10^9 \,\mathrm{M}_{\odot}}\right)^{-1/3} m_{22}^{-1},$$
 (5)

where  $M_h$  uses the Bryan & Norman (1998) definition of virial mass. Together, equations (3) and (5) imply that

$$\rho_c = 2.94 \times 10^6 \text{ M}_{\odot} \text{kpc}^{-3} \left(\frac{M_h}{10^9 \text{ M}_{\odot}}\right)^{4/3} m_{22}^2.$$
 (6)

If we define the soliton core mass as  $M_c \equiv 4\pi \rho_c r_c^3/3$  then we have

$$M_{\rm c} = 5.04 \times 10^7 \,\mathrm{M}_{\odot} \left(\frac{M_{\rm h}}{10^9 \,\mathrm{M}_{\odot}}\right)^{1/3} m_{22}^{-1} \,.$$
 (7)

One implication of these relations is that the smallest haloes will have the largest soliton core radii and lowest density soliton cores. Also, as halo mass increases, the soliton core size as a fraction of virial radius becomes insignificant  $r_{\rm c}/r_{\rm vir} \propto M_{\rm h}^{-2/3}$ :

$$\frac{r_{\rm c}}{r_{\rm vir}} = 6.20 \times 10^{-2} \left(\frac{M_{\rm h}}{10^9 \,{\rm M}_{\odot}}\right)^{-2/3} m_{22}^{-1} \,.$$
 (8)

Similarly, the fraction of a halo's mass locked up in the soliton core decreases rapidly with halo mass  $M_c/M_h \propto M_h^{-2/3}$ :

$$\frac{M_{\rm c}}{M_{\rm h}} = 5.04 \times 10^{-2} \left(\frac{M_{\rm h}}{10^9 \,\mathrm{M}_{\odot}}\right)^{-2/3} m_{22}^{-1} \,. \tag{9}$$

The ratio of the circular velocities at the core and virial radius does not depend on either  $M_h$  or m:  $V_c(r_c)/V_c(r_{vir}) \sim 0.9$ .

Finally, we note that the product  $r_c M_c$  is independent of halo mass:

$$r_{\rm c} M_{\rm c} = 8.06 \times 10^7 \, m_{22}^{-2} \, {\rm M}_{\odot} \, {\rm kpc} \,.$$
 (10)

Equation (10) means that the specific angular momentum of an object on a circular orbit within the soliton core depends only on the scalar field mass, not on the halo mass itself:  $j_c = \sqrt{G r_c M_c} = 18.6 m_{22}^{-1}$  kpc km s<sup>-1</sup>. This is very similar to the characteristic angular momentum scale of the quantum field,  $\hbar/m = 19 m_{22}^{-1}$  kpc km s<sup>-1</sup>.

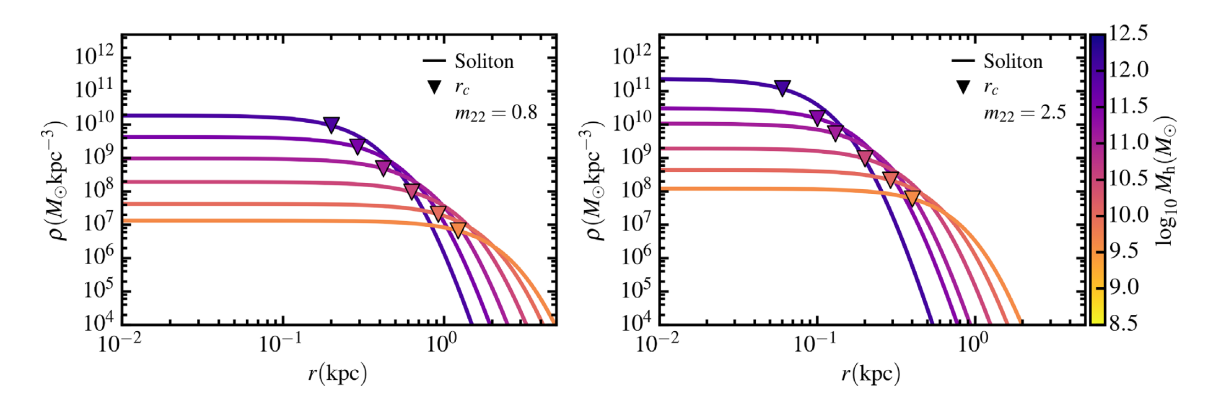


Figure 2. Density profiles for the soliton cores in SFDM haloes according to equations (5) and (6). Results are shown for scalar field masses of  $m = 8 \times 10^{-23}$  eV (left) and  $m = 5 \times 10^{-22}$  eV (right). The core radius for each soliton is marked as a triangle. The colour code is matched to halo virial mass (see colourbar at right). For a fixed scalar field particle mass m, lower mass haloes have larger soliton cores with lower overall density. At fixed halo mass, the solitons are less dense and have larger radii for lighter bosons. Note that the outer dark matter envelope that is expected to surround each soliton is not shown in this figure.

Fig. 2 uses equations (2), (5), and (6) to show the central soliton profiles for SFDM haloes over a range of virial masses (colour bar). The left- and right-hand panels assume scalar field masses of  $m_{22} = 0.8$  and  $m_{22} = 2.5$ , respectively. Note that for  $m_{22} = 0.8$  (2.5), haloes smaller than  $M_h \sim 10^{9.5} (10^{8.5}) M_{\odot}$  are unstable due to the quantum pressure and may not form, therefore haloes below these masses are not plotted.

We note that although the precise factors in equations (5) and (6) are empirical, being best-fitting values for the cosmological simulations of Schive et al. (2014); we will assume these values for the rest of our derivation. A study of how these values vary in different numerical implementations is out of the scope of this work.

# 2.2 The outer envelope

We aim to define a complete SFDM density profile given a particle mass  $m_{22}$  and a halo mass  $M_h$ . Schive et al. (2014) found that the soliton profile in equation (2) was only a good fit for  $r \le \alpha r_c \simeq 3 r_c$ . Beyond this radius, the solitonic cores were seen to transition to a CDM-like profile similar to the (Navarro et al. 1997) form

$$\rho_{\rm NFW}(r) = \frac{\rho_{\rm s}}{(r/r_{\rm s})(1 + r/r_{\rm s})^2},\tag{11}$$

where  $r_s$  is the radius where the logarithmic slope of the density profile is -2.

A natural way to model an SFDM halo out to  $r_{\rm vir}$  is to transition from the soliton profile (2) to an NFW profile (11) at some specified radius  $r_{\alpha}$ . Several authors have followed this approach (Marsh & Silk 2014; González-Morales et al. 2017; Bernal et al. 2018); however, past choices for the transition radius were not based on simulation results but rather relied on the estimate  $r_{\alpha} = r_{\rm c}$  or finding the point where the density log-slopes are equal. However, SFDM haloes in simulations (Schive et al. 2014; Mocz et al. 2017) all show a transition radius several times larger than  $r_{\rm c}$  and reveal that the density slopes can differ significantly at the transition point. Specifically, the transition from solitonic core to NFW profile is sharp, with the soliton almost superimposed on top of the NFW.

Furthermore, SFDM simulations do not predict a unique transition radius due to the turbulence in the field (Schive et al. 2014; Schwabe et al. 2016; Veltmaat & Niemeyer 2016). The difficulty in providing a single profile for the total halo has recently led to more complex assumptions. For instance, Lin et al. (2018) adopted a mode decomposition of the scalar field wave function that comes

from simulations of Schive et al. (2014). The authors fit the inferred distribution function from simulations to various classical particle distribution functions and found that the fermionic King model (Chavanis 1998) provided a good fit. A different approach was given in Bar et al. (2018), who reinterpret equation (5) as a statement that the energy per unit mass of the soliton is equal to that of the total halo and develop their analysis under this assumption.

We will follow a phenomenological approach to link the inner halo with the outer halo. To capture the features observed in SFDM simulations and account for the (relatively small) variations in the transition radius for a given halo mass, we explore a range of radii that mark the transition from soliton to outer halo:

$$r_{\alpha} = \alpha \, r_{\rm c} \,. \tag{12}$$

With this choice, the total density profile is

$$\rho(r) = \begin{cases} \rho_{\text{sol}}(r) & 0 \le r \le r_{\alpha} \\ \rho_{\text{NFW}}(r) & r_{\alpha} \le r \le r_{\text{vir}}. \end{cases}$$
 (13)

We now must fix two parameters for both the inner soliton piece and outer NFW piece in equation (13). Given  $m_{22}$  and  $M_h$ , equations (2), (5), and (6) define the  $\rho_{sol}(r)$  completely. For the outer NFW piece (equation 11), we need two additional constraints in order to set  $\rho_s$  and  $r_s$ . For these, we impose density continuity at  $r_\alpha$ 

$$\rho_{\text{sol}}(r_{\alpha}) = \rho_{\text{NFW}}(r_{\alpha}), \tag{14}$$

and mass conservation within  $r_{\rm vir}$ 

$$\begin{split} M_{\rm h} &= 4\pi \int_0^{r_{\rm vir}} \rho(r') r'^2 \, \mathrm{d}r' \\ &= 4\pi \int_0^{r_{\alpha}} \rho_{\rm sol}(r') r'^2 \, \mathrm{d}r' + \int_{r_{\alpha}}^{r_{\rm vir}} \rho_{\rm NFW}(r') r'^2 \, \mathrm{d}r'. \end{split} \tag{15}$$

By assuming mass conservation, we are explicitly assuming that the quantum pressure is not sufficient to result in the existence of significant additional mass beyond the virial radius compared to CDM. This should be a reasonable approximation for all but the smallest haloes (with halo masses just above the suppression mass for a given m).

We emphasize that the outer NFW profile of the SFDM halo will not necessarily track the NFW profile for the same mass halo in CDM. The effective concentration ( $c = r_{\rm vir}/r_{\rm s}$ ) and normalization of the two NFW haloes can be different because a non-negligible portion of the SFDM halo mass may be locked up within the central soliton. Of course, the global structure of CDM haloes informs what

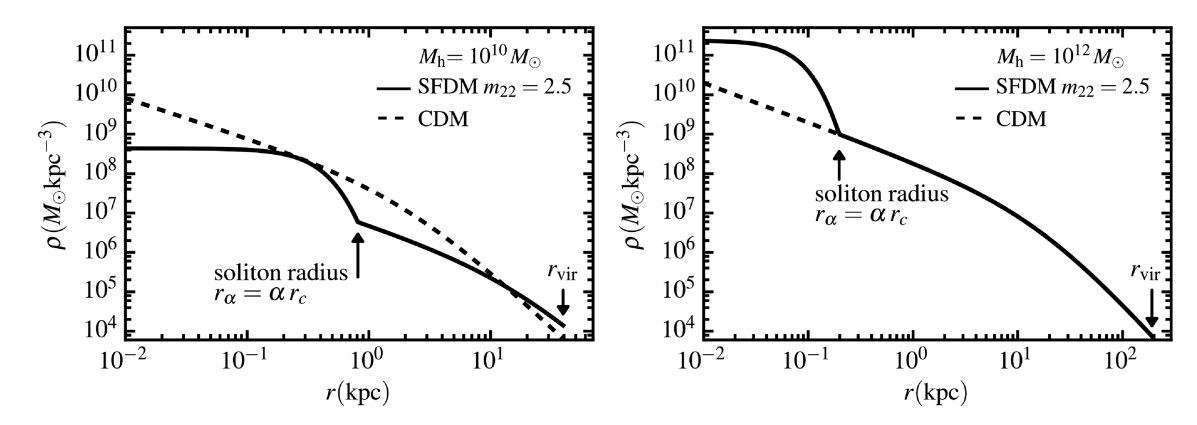


Figure 3. SFDM (solid, with  $m_{22}=2.5$ ) and CDM (dashed) profiles shown for a a dwarf-size halo ( $M_h=10^{10} \, \mathrm{M_{\odot}}$ , left) and a Milky Way size halo ( $M_h=10^{12} \, \mathrm{M_{\odot}}$ , right). The SFDM halo transitions from soliton to NFW at  $r_{\alpha}\equiv \alpha \, r_c$  with  $\alpha=2$  and 3 on the left and right, respectively (see the text for details). In both cases, the soliton transition is sharp, in agreement with simulations (Schive et al. 2014; Mocz et al. 2017). The soliton core is large and of lower density than the CDM case in the dwarf halo. In the Milky Way halo, the soliton is denser than the CDM halo at radii  $r \lesssim r_c$ .

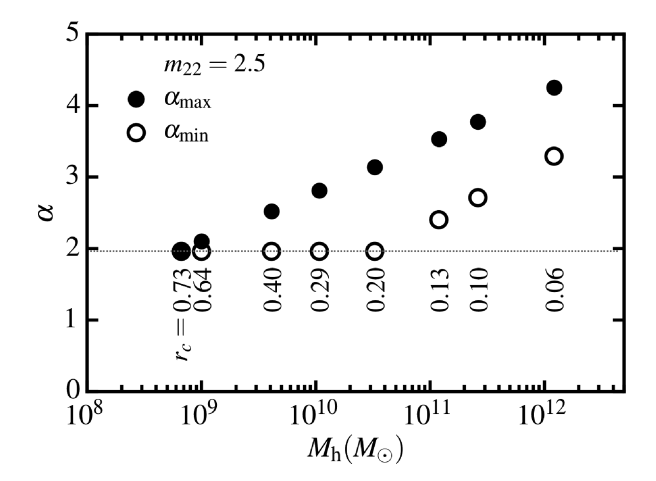
is plausible for SFDM haloes in that we generally expect the mass and potential well depth at the virial radius to be similar when  $\lambda_{\rm dB} \ll r_{\rm vir}$ . Fortunately, CDM halo concentrations are well understood from cosmological simulations (e.g. Bullock et al. 2001). In what follows, we assume the Planck Collaboration XXIII (2015) cosmology and the concentration—mass relation from Dutton & Macciò (2014) to determine the CDM prediction.

Fig. 3 shows example profiles for a Milky Way size halo (right) and a dwarf-size halo (left) for characteristic choices of  $\alpha$  motivated below (3 and 2, respectively). We adopt  $m_{22}=2.5$  in this example. Note the difference between CDM and SFDM is largest for the dwarf halo. This will generally be the case: the fractional mass contained within the soliton core increases with decreasing halo mass. Indeed, the soliton core in the dwarf halo is less dense than the CDM cusp and has a size comparable to the half-light radius of a classical dwarf spheroidal ( $\sim$ 500 pc). Conversely, the soliton in a Milky-Way-like system at a radius of  $r_{\rm c} \sim 100$  pc is even denser than CDM; such a halo has a very similar density in SFDM and CDM at a typical half-light radius for a Milky Way size galaxy ( $r_{\rm gal} \sim 3$  kpc).

Cosmological SFDM simulations find values of  $\alpha \sim 3$ , though these simulations exist only for haloes in a limited mass range  $M_{\rm h} \sim 10^{11}\,{\rm M}_{\odot}$  (Schive et al. 2014). Idealized simulations suggest that the transition occurs approximately at the radius where the potential energy density is comparable to the total quantum kinetic energy density (Mocz et al. 2017). The value of  $\alpha$  can be modified by constructive and destructive interference of the intrinsic phase of the soliton with the uncorrelated phases of the surrounding medium. Our goal is to define a range of  $\alpha$  values that are plausible at each halo mass scale.

We bracket minimum ( $\alpha_{\min}$ ) and maximum ( $\alpha_{\max}$ ) soliton transition radii by imposing several simple constraints on the circular velocity profile. These constraints are motivated by simulation results and physical plausibility. First, we demand that the soliton produces a local maximum in the circular velocity curve  $V_c(r)$  at a radius  $r \sim r_c$ . Secondly, we ensure that the global circular velocity curve of the SFDM halo has a maximum that does not exceed its CDM counterpart (qualitatively that the potential well is never deeper than it would be in CDM). Finally, we demand that the radius where maximum circular velocity of the halo occurs  $r_{\max}$  is within  $r_{\text{vir}}$ .

Fig. 4 shows the range of  $\alpha$  values that are allowed by our conditions as a function of halo mass. For low-mass haloes, the condition



**Figure 4.** Range of soliton transition radii allowed as a function of halo mass parameterized by  $\alpha$ , where the transition radius is  $r_{\alpha} \equiv \alpha r_{c}$  and  $r_{c}$  is the soliton core radius (see equations 12 and 13). The numbers show the value of  $r_{c}$  in units of kpc for several halo masses.

that matters most in setting  $\alpha_{\min}$  is the existence of a gravitationally dominant soliton (a local maximum in  $V_c(r)$ ). For larger haloes  $(M_h \gtrsim 10^{11}\,\mathrm{M}_\odot)$ ,  $\alpha_{\min}$  is set by demanding  $V_{\max}^{\mathrm{SFDM}} \leq V_{\max}^{\mathrm{CDM}}$ . For haloes of all masses,  $\alpha_{\max}$  is set by the condition  $r_{\max} \leq r_{\mathrm{vir}}$ . In a dwarf-size halo  $(M_h \sim 10^{10}\,\mathrm{M}_\odot)$ , the  $\alpha$  range is  $\sim 2$ –3. In Milky Way mass haloes, the  $\alpha$  range is  $\sim 3$ –4. For reference, the size of the soliton core expected at each halo mass (in kpc) is displayed below the  $\alpha=2$  line in Fig. 4. Note that even though  $\alpha$  values are slightly larger for more massive haloes, the value of  $r_c$  decreases even faster, meaning that the physical extent of the soliton-dominated region  $(\alpha r_c)$  decreases with increasing halo mass. <sup>1</sup>

Fig. 5 provides examples of how SFDM halo profiles (left) and circular velocity curves (right) differ from CDM expectations for three example halo masses: a Milky Way ( $M_h = 10^{12} \, \mathrm{M}_{\odot}$ , top),

<sup>&</sup>lt;sup>1</sup>Note that while we naively expect similar scaling to even higher masses associated with galaxy clusters, these haloes experience more recent mergers and are more dynamically influenced by large sub-structures. Quantum interference is therefore likely more intricate in these systems. Cosmological simulations at these higher mass scales will be required before we are able to make confident predictions.

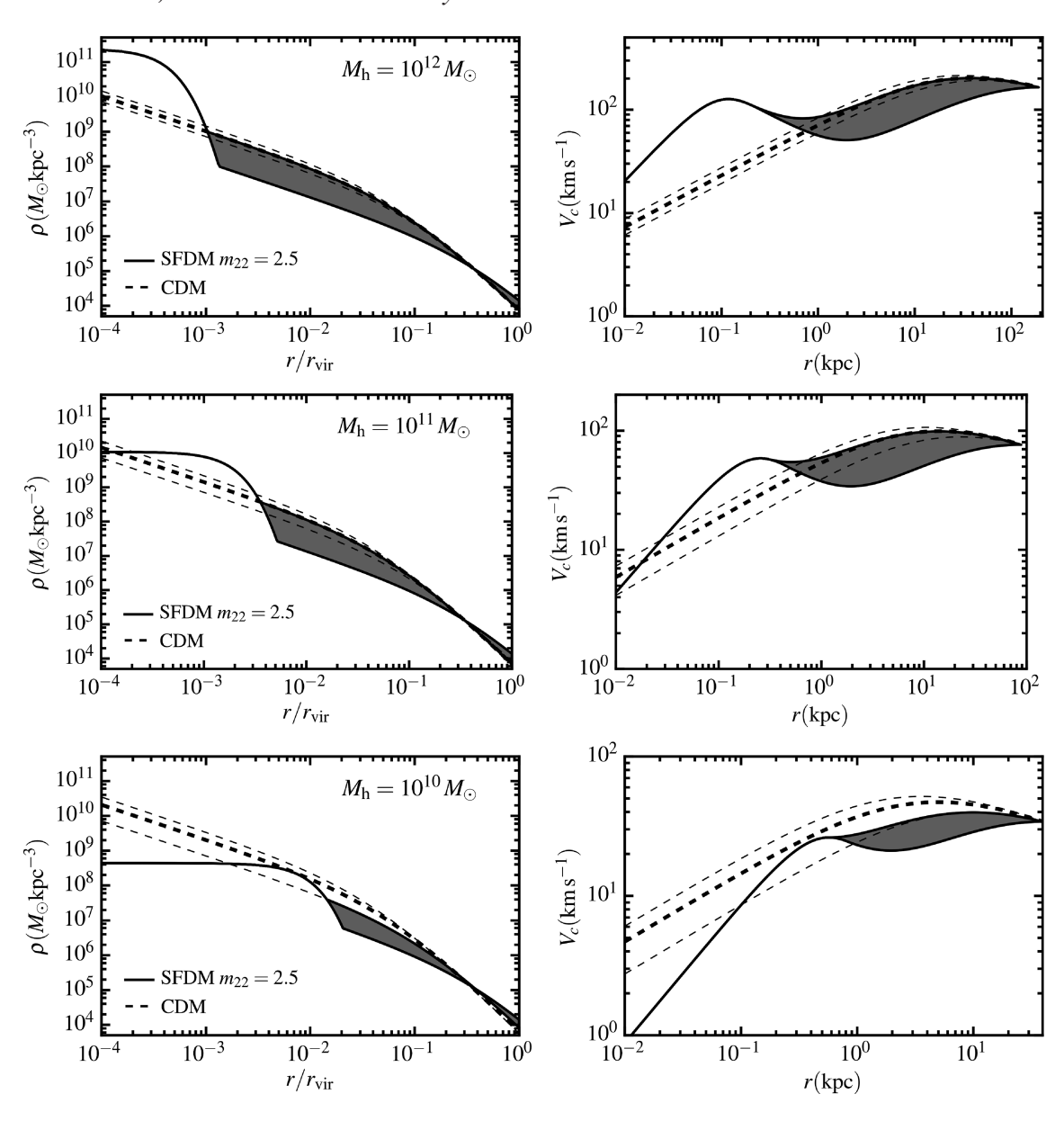


Figure 5. Density profiles (left) and rotation curves (right) for SFDM (solid) and CDM (dashed) haloes of three example masses:  $M_h = 10^{12}$  (top),  $10^{11}$  (middle), and  $10^{10}$  (bottom)  $M_{\odot}$ . The light-dashed CDM lines show  $\pm 1\sigma$  scatter in the halo concentrations at fixed halo mass (Macciò, Dutton & Van Den Bosch 2008). The density profiles are shown as a function of radius normalized by the halo virial radius in order to emphasize that the size of the soliton core is proportionally larger in the lower mass haloes. The associated circular velocity curves (right) are plotted as a function of unnormalized radius to provide a sense of the physical scale. The shaded regions in the SFDM profiles allow for a range of soliton transition radii ( $r_{\alpha} = \alpha r_{c}$ , see Fig. 3). In the smallest haloes, the minimum soliton size ( $\alpha_{min}$ ) is set by demanding a local maximum in the circular velocity curve (lower right panel). In the largest haloes,  $\alpha_{min}$  is set by demanding that the peak circular velocity within the soliton does not exceed the global circular velocity of the halo (upper right). For all masses, the maximum soliton radius is set by requiring that the maximum circular velocity is reached within  $r_{vir}$ .

a small spiral ( $M_h = 10^{11} \, \mathrm{M}_\odot$ , middle), a dwarf galaxy ( $M_h = 10^{10} \, \mathrm{M}_\odot$ , bottom). In the left-hand panels, we plot the density as a function of  $r/r_{\rm vir}$ . In the right-hand panels, radii are ploted in physical (unscaled) units. In each case, solid lines correspond to SFDM and dashed lines to CDM. The shaded regions in the SFDM haloes span  $\alpha_{\rm min}$  to  $\alpha_{\rm max}$ . Note that in the smallest haloes, the soliton dominates within an appreciable ( $\sim 1$  per cent) fraction of the virial radius and has a lower core density than CDM. For larger haloes, however, the soliton can be as small as  $\sim 0.1$  per cent of the virial radius and its density is larger than the CDM halo in

this region. For dwarf-size haloes, SFDM circular velocity curves are expected to lie below and rise more quickly than corresponding  $V_{\rm c}(r)$  in CDM; for hosts of  $V_{\rm c}\sim 100$ –200 km s<sup>-1</sup> galaxies, SFDM haloes are both denser and more peaked at small radii than CDM. This unique behaviour may provide a means to discriminate between the theories: it is substantially different from what is found in other alternative dark matter models, where the core region is generally less dense than the density of a CDM halo of the same virial mass (see Robles et al. 2017, and references therein).

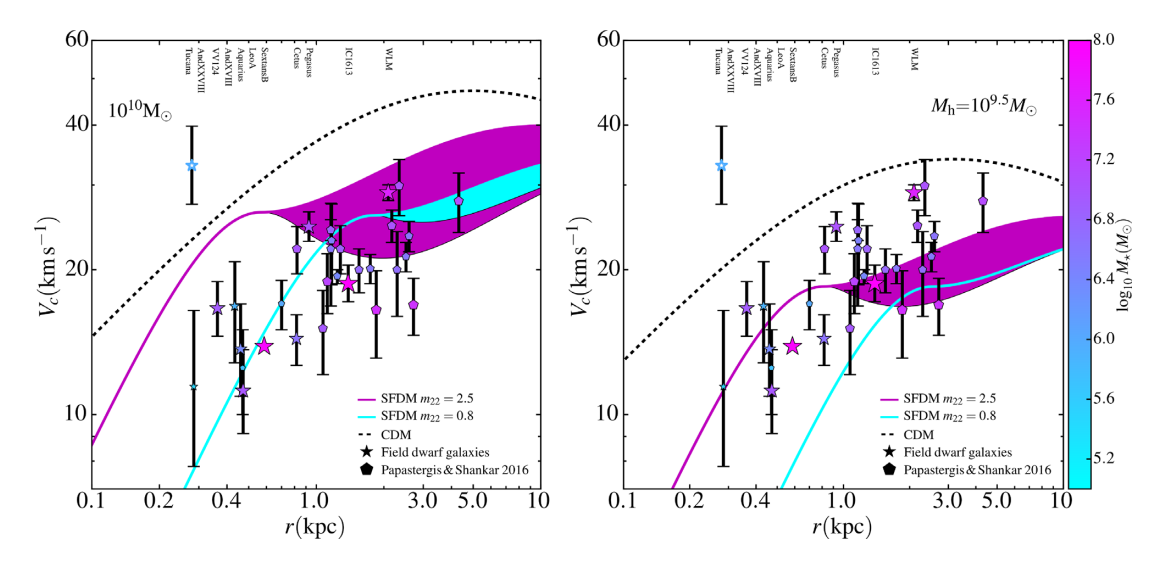


Figure 6. TBTF halo comparison for CDM (dashed) and SFDM (magenta for  $m_{22} = 2.5$  and cyan for  $m_{22} = 0.8$ ). Stars show half-light circular velocities for non-satellite Local Group dwarf galaxies and pentagons show isolated field dwarf galaxies. Symbol sizes and colours vary with galaxy stellar mass as indicated by the colourbar. The two panels compare CDM and SFDM predictions at fixed halo mass of  $M_h = 10^{10} \, \mathrm{M_{\odot}}$  (left) and  $M_h = 10^{9.5} \, \mathrm{M_{\odot}}$  (right), which are typical of TBTF haloes. The CDM predictions (at median concentration) are too dense relative to observations, as expected. The SFDM haloes are a better match to the densities of observed galaxies; this is particularly notable at large radii (well beyond the galaxies' half-light radii), where baryonic feedback is less effective at producing cores in CDM haloes.

# 3 COMPARISON WITH GALAXY DATA

#### 3.1 The too big to fail problem and SFDM haloes

As originally cast, the TBTF problem with CDM (DM-only) simulations refers to the fact that the central densities of the most massive sub-haloes in a Galaxy-size hosts are higher than the central densities observed in dwarf galaxies of the Milky Way (Boylan-Kolchin et al. 2011; Boylan-Kolchin, Bullock & Kaplinghat 2012) and Andromeda (Kirby et al. 2014; Tollerud, Boylan-Kolchin & Bullock 2014). A related problem exists for galaxies in the Local Group that are not satellites of larger hosts (Garrison-Kimmel et al. 2014) and for dwarf galaxies in the field (Ferrero et al. 2012; Papastergis et al. 2015; Papastergis & Shankar 2016). The second incarnation associated with non-satellite galaxies is regarded as more problematic. This is because satellite sub-haloes are likely to end up less dense than seen in DM-only simulations owing to enhanced mass loss associated with the central Galaxy potential (Zolotov et al. 2012; Garrison-Kimmel et al. 2018). Field haloes do not experience enhanced mass loss of this kind and are thus more robust to the inclusion of baryonic effects in simulations.

Fig. 6 explores the extent to which SFDM may alleviate the TBTF problem in the field. We show the circular velocities of  $M_{\rm h}=10^{9.5}\,{\rm M}_{\odot}$  haloes (right-hand panel) and  $10^{10}\,{\rm M}_{\odot}$  haloes (left) in SFDM (magenta for  $m_{22}=2.5$  and cyan for  $m_{22}=0.8$ ) and CDM (at median concentration, dashed). These halo masses are similar to those required to match the local counts of  $M_{\star}\simeq 10^6{\rm M}_{\odot}$  dwarf galaxies and are the relevant scale for TBTF comparisons (Bullock & Boylan-Kolchin 2017). The associated scatter in the outer mass distribution due to the variations in  $\alpha$  is captured by the shaded regions.

The star-shaped data points show circular velocities measured at the half-light radii of non-satellite Local Group galaxies as compiled by Garrison-Kimmel et al. (2014).<sup>2</sup> Circular velocities of isolated dwarf galaxies measured out to larger radii from Papastergis & Shankar (2016) are shown as pentagons. The points are colour coded by galaxy stellar mass using the colourbar to the right. The colourbar reflects galaxy stellar mass. Note that haloes of galaxies smaller than  $M_{\star} \simeq 5 \times 10^6 \mathrm{M}_{\odot}$  are expected to be only marginally affected by feedback (e.g. Fitts et al. 2017).

The SFDM circular velocity profiles are always below those of CDM in Fig. 6 and are generally in better agreement with the data, alleviating the TBTF problem in the field. In particular, the SFDM models are even able to accommodate the Papastergis & Shankar (2016) data, which probe the outer radii of galaxies ( $\gtrsim$  1 kpc) beyond the stellar half-light radius. These are regions where hydrodynamic simulations have difficulty lowering the densities of CDM haloes, even with strong feedback (Tollet et al. 2016; Fitts et al. 2017). We conclude from this comparison that SFDM provides a possible solution to the TBTF problem with some potential advantages to CDM + feedback models.

# 3.2 The central density problem and SFDM haloes

The cusp/core problem in CDM refers to the tendency for measured rotation curves of dark-matter-dominated galaxies to favour fits that imply centrally cored ( $\rho \sim \text{constant}$ ) dark matter density profiles as opposed to NFW-like cusps with  $\rho \propto r^{-1}$  (McGaugh, Rubin & de Blok 2001; Simon et al. 2005; de Blok et al. 2008; Kuzio de Naray, McGaugh & de Blok 2008). A related issue is that rotation curves indicate lower central densities than pre-

<sup>&</sup>lt;sup>2</sup>The data are from Kirby et al. (2014), Hoffman et al. (1996), Simon & Geha (2007), Epinat et al. (2008), Fraternali et al. (2009), and Collins et al. (2013).

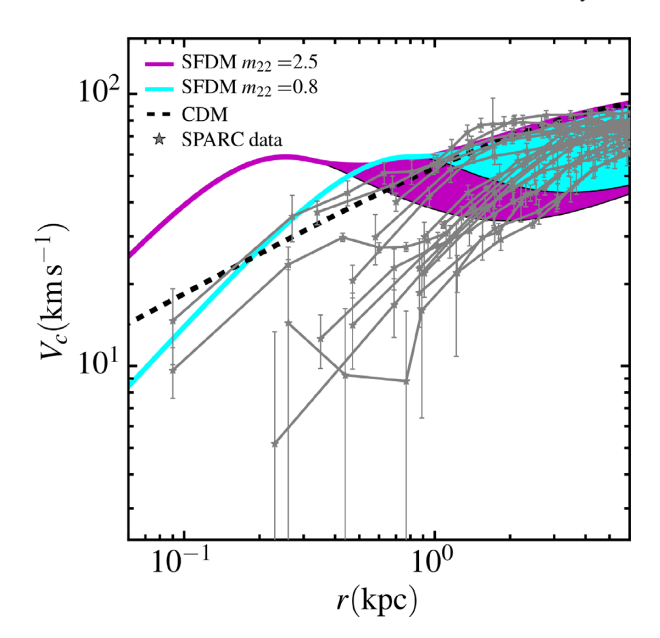


**Figure 7.** Circular velocities of galaxies from the SPARC database chosen to have asymptotic velocities in the range  $80-100\,\mathrm{km\,s^{-1}}$  (gray stars connected by thin lines). We include only the dark matter component assuming a stellar mass-to-light ratio of 0.2. These are compared to predicted rotation curves for  $M_{\rm h}=10^{11}\,\mathrm{M}_{\odot}$  haloes in CDM (dashed) and SFDM (solid). We show SFDM predictions for two scalar field masses,  $m_{22}=2.5$  (magenta) and  $m_{22}=0.8$  (cyan). While most of the data at  $r>1\,\mathrm{kpc}\sim r_{\rm gal}$  are within the expected scatter for this halo mass in SFDM, the observed rotation velocities at smaller radii are generally lower than those predicted in CDM and SFDM. The SFDM models are *more* discrepant with the data than CDM at small radii, exacerbating the central-density and cusp/core problem.

dicted in CDM (Alam, Bullock & Weinberg 2002; Oman et al. 2015). A circular velocity scale that is of particular interest for comparison to SFDM models is  $\sim 100 \text{ km s}^{-1}$ , as these haloes  $(M_h \simeq 10^{11} \text{ M}_{\odot})$  are massive enough to have dense soliton cores but small enough that we observe low-density cores in their associated galaxies.

In Fig. 7, the gray stars connected by thin gray solid lines show galaxy rotation curves from the SPARC database of galaxy rotation curves (Lelli, McGaugh & Schombert 2016), specifically the 17 with asymptotic velocities in the range 80–100 km s<sup>-1</sup>. An important consideration when inferring the inner rotation curve directly from gas kinematics is the observational uncertainty coming from effects including beam smearing, complicated gas morphology, and bars, as this may affect the central mass estimation (Corbelli & Walterbos 2007; Pizzella et al. 2008; Kam et al. 2015). The SPARC database does include corrections for observational uncertainties. The comprehensive analysis of Lelli et al. (2016) found that beam smearing effects, local non-circular motions, and global kinematic asymmetries related to define the centre of rotation or inclination errors are small and do not significantly affect the rotation curves for the galaxy sample shown in Fig. 7. The largest uncertainty was the stellar mass-light-ratio at 3.6 µm; Lelli et al. (2016) explored two cases for the average value, 0.2 and 0.5, and found that a value of 0.5 is in better agreement with the full SPARC data. It also agrees with stellar population synthesis models (McGaugh & Schombert 2014; Meidt et al. 2014), resolved stellar populations in the LMC (Eskew, Zaritsky & Meidt 2012), and the BTFR (McGaugh & Schombert 2015). We have subtracted the gas and disc components from observed rotation curves by assuming a single stellar mass-to-light ratio of 0.2 for all the galaxies at  $3.6\,\mu m$  (see the discussion in section 5.1 of Lelli et al. 2016). This value provides the minimal contribution allowable from stars to the rotation curve; increasing the stellar mass-to-light ratio to 0.4 will overall decrease slightly the rotation curves but will not modify our main conclusion.

For comparison, we show the predicted rotation curves for  $M_{\rm h}=10^{11}\,{\rm M}_{\odot}$  haloes in CDM (black dash) and SFDM (solid) with  $m_{22}=2.5$  (magenta) and  $m_{22}=0.8$  (cyan). 14 of the 17 galaxies plotted show a decrement in central rotational velocity compared to the CDM expectation, which is characteristic of the cusp/core problem. Importantly, however, the mismatch at small radii is even worse in the SFDM models owing to the high density of solitons expected at this circular velocity scale. Conversely, the diversity (Oman et al. 2015) in the data at larger radii ( $\sim$ 2 kpc) is potentially more easily accommodated in SFDM models. We note that significantly smaller scalar field masses ( $m_{22}<0.8$ ) would better fit the inner regions of the SPARC data at this velocity scale, consistent with the results of Bernal et al. (2018); however, masses this small are ruled out by cosmological constraints (Bozek et al. 2015; Sarkar et al. 2016).

One important take away from Fig. 7 is that viable SFDM models do *not* solve the central density problem or cusp/core problem prevalent in  $\sim 100 \; \mathrm{km} \, \mathrm{s}^{-1}$  galaxies. If anything, SFDM exacerbates the issue [provided equation (5) is valid]. This suggests that both SFDM and CDM require some baryonic feedback mechanism to reduce the central densities of haloes at this mass scale.

#### 4 CONCLUSIONS

We have presented an analytical formalism for predicting dark matter halo profile structure in SFDM models in which the dark matter particle mass is so small ( $m \sim 10^{-22}$  eV) that quantum phenomena are important on astrophysically relevant scales ( $\sim$ 1 kpc). This model, known alternatively as Bose–Einstein condensate dark matter, ultralight dark matter, WDM,  $\psi$ DM, and fuzzy dark matter, has gained relevance given its potential for solving some of the small-scale problems in cosmology (Hu et al. 2000; Matos et al. 2000; Robles & Matos 2012; Hui et al. 2017; Suárez & Chavanis 2017). In view of the demanding spatial resolution required to follow the quantum interference at different scales in SFDM cosmological simulations, our approach offers a useful alternative to describe haloes at all masses and at all radii at z=0. Additionally, it can be applied to any scalar field mass m.

As summarized in Section 2.1, our approach builds upon the results of Schive et al. (2014), who used cosmological simulations to parameterize soliton core sizes  $r_c$  and densities as a function of halo virial mass  $M_h$ . Importantly, the soliton cores are largest (and lowest density) in the smallest haloes, as might be expected from the uncertainty principle:  $r_c \sim \lambda_{\rm dB} \propto m^{-1} v^{-1} \propto m^{-1} \, M_h^{-1/3}$ . The soliton regions transition to an outer profile that mirrors CDM expectations in the regime where quantum pressure is negligible. We parameterize the transition radius  $r_\alpha = \alpha \, r_c$  with a range of  $\alpha$  values that are plausible and that characterize the expected range where the soliton transitions from a turbulent region to the dust-like CDM halo (see Section 2.2). Assuming the validity of equation (5), the central regions of SFDM haloes will be dominated by solitons that are denser than the same halo in CDM at masses above  $M_h \sim 10^{10.5} \, M_{\odot}$  (see e.g. Fig. 5).

Using our formalism, we consider the smallest SFDM masses  $(m = 0.8 - 2.5 \times 10^{-22} \text{ eV})$  that are still consistent with large-scale structure constraints, as such models will result in manifestations of quantum pressure (solitons) on the largest astrophysical scales. In

such models, dwarf-size dark matter halos ( $M_h \sim 10^{10}~M_\odot$ ) have lower central densities than their CDM counterparts, alleviating the TBTF problem in a regime where feedback is less effective (see Fig. 6). However, the cusp/core problem seen in more massive ( $M_h \sim 10^{11} M_\odot$ ) dwarf galaxies is exacerbated. We use rotation curves of  $\sim 100~km~s^{-1}$  galaxies from the SPARC database to show that SFDM halos are denser at the radii where rotation curves rise than even cuspy NFW haloes. This makes the low central densities observed in dark matter dominated galaxies even harder to understand in SFDM models than in CDM (Fig. 7). For Milky Way mass haloes, SFDM has a soliton density well above the CDM expectation at  $\sim 100~pc$ , some  $\sim 10~times$  denser than the equivalent NFW profile at those radii (see also Bar et al. 2018).

Our results motivate future large-scale SFDM simulations in order to confirm the predicted soliton scalings with halo mass and to explore the expected scatter in transition radii from soliton to NFW-like envelopes. Updated scalings (e.g. an updated form of equation 5) can be easily accommodated in our approach. They also motivate the need to incorporate hydrodynamics and star-formation feedback into SFDM simulations in order to determine whether or not baryonic processes can alleviate the core-density tension for SFDM highlighted in Fig. 7. If not, then one of the classic small-scale problems that originally motivated SFDM may be its undoing.

# **ACKNOWLEDGEMENTS**

VHR acknowledges support from the University of California Institute for Mexico and the United States and Mexico's National Council for Science and Technology (CONACYT) through the postdoctoral fellowship. This work was also supported by the National Science Foundation (NSF) grants AST-1518291 and PHY-1620638 and by the National Aeronautics and Space Administration (NASA) through Hubble Space Telescope (HST) theory grants (programs AR-13921, AR-13888, and AR-14282) awarded by the Space Telescope Science Institute (STScI), which is operated by AURA, Inc., under NASA contract NAS5-26555. MBK also acknowledges support from NSF grant AST-1517226 and CA-REER grant AST-1752913 and from NASA grants NNX17AG29G and HST-AR-13896, HST-AR-14554, HST-AR-15006, HST-GO-12914, and HST-GO-14191 from STScI.

#### REFERENCES

Alam S. M. K., Bullock J. S., Weinberg D. H., 2002, ApJ, 572, 34
Amendola L., Barbieri R., 2006, Phys. Lett. B, 642, 192
Balakrishna J., Seidel E., Suen W.-M., 1998, Phys. Rev. D, 58, 104004
Bar N., Blas D., Blum K., Sibiryakov S., 2018, Phys. Rev D, 98, 083027.
Bernal T., Robles V. H., Matos T., 2017, MNRAS, 468, 3135
Bernal T., Fernández-Hernández L. M., Matos T., Rodríguez-Meza M. A., 2018, MNRAS, 475, 1447

Bode P., Ostriker J. P., Turok N., 2001, ApJ, 556, 93
Böhmer C. G., Harko T., 2007, J. Cosmol. Astropart. Phys., 2007, 025
Bond J. R., Szalay A. S., Turner M. S., 1982, Phys. Rev. Lett., 48, 1636
Boylan-Kolchin M., Bullock J. S., Kaplinghat M., 2011, MNRAS, 415, L40
Boylan-Kolchin M., Bullock J. S., Kaplinghat M., 2012, MNRAS, 422, 1203
Bozek B., Marsh D. J. E., Silk J., Wyse R. F. G., 2015, MNRAS, 450, 209
Bozek B., Boylan-Kolchin M., Horiuchi S., Garrison-Kimmel S., Abazajian K., Bullock J. S., 2016, MNRAS, 459, 1489

Brooks A. M., Kuhlen M., Zolotov A., Hooper D., 2013, ApJ, 765, 22 Bryan G. L., Norman M. L., 1998, ApJ, 495, 80

Bullock J. S., Boylan-Kolchin M., 2017, ARA&A, 55, 343

Bullock J. S., Kolatt T. S., Sigad Y., Somerville R. S., Kravtsov A. V., Klypin A. A., Primack J. R., Dekel A., 2001, MNRAS, 321, 559

Calabrese E., Spergel D. N., 2016, MNRAS, 460, 4397

Chan T. K., Kereŝ D., Oñorbe J., Hopkins P. F., Muratov A. L., Faucher-Giguère C.-A., Quataert E., 2015, MNRAS, 454, 2981

Chavanis P.-H., 1998, MNRAS, 300, 981

Chavanis P.-H., 2011, Phys. Rev. D, 84, 043531

Chavanis P.-H., 2016, Phys. Rev. D, 94, 083007

Chavanis P. H., 2012, A&A, 537, A127

Chen S.-R., Schive H.-Y., Chiueh T., 2017, MNRAS, 468, 1338

Collins M. L. M. et al., 2013, ApJ, 768, 172

Corbelli E., Walterbos R. A. M., 2007, ApJ, 669, 315

de Blok W. J. G., Walter F., Brinks E., Trachternach C., Oh S.-H., Kennicutt R. C., Jr, 2008, AJ, 136, 2648

Di Cintio A., Brook C. B., Macciò A. V., Stinson G. S., Knebe A., Dutton A. A., Wadsley J., 2014, MNRAS, 437, 415

Dutton A. A., Macciò A. V., 2014, MNRAS, 441, 3359

Elbert O. D., Bullock J. S., Garrison-Kimmel S., Rocha M., Oñorbe J., Peter A. H. G., 2015, MNRAS, 453, 29

Epinat B. et al., 2008, MNRAS, 388, 500

Eskew M., Zaritsky D., Meidt S., 2012, AJ, 143, 139

Ferrero I., Abadi M. G., Navarro J. F., Sales L. V., Gurovich S., 2012, MNRAS, 425, 2817

Fitts A. et al., 2017, MNRAS, 471, 3547

Flores R. A., Primack J. R., 1994, ApJ, 427, L1

Fraternali F., Tolstoy E., Irwin M. J., Cole A. A., 2009, A&A, 499, 121

Garrison-Kimmel S. et al., 2018, preprint (arXiv:1806.04143)

Garrison-Kimmel S., Rocha M., Boylan-Kolchin M., Bullock J. S., Lally J., 2013, MNRAS, 433, 3539

Garrison-Kimmel S., Boylan-Kolchin M., Bullock J. S., Kirby E. N., 2014, MNRAS, 444, 222

Gleiser M., 1988, Phys. Rev. D, 38, 2376

Gleiser M., Watkins R., 1989, Nucl. Phys. B, 319, 733

González-Morales A. X., Marsh D. J. E., Peñarrubia J., Ureña López L. A., 2017, MNRAS, 472, 1346

González-Samaniego A., Avila-Reese V., Colín P., 2016, ApJ, 819, 101

Governato F. et al., 2012, MNRAS, 422, 1231

Guo H. et al., 2016, MNRAS, 459, 3040

Guzmán F., Ureña López L., 2006, ApJ, 645, 814

Guzmán F. S., Ureña López L. A., 2004, Phys. Rev. D, 69, 124033

Hlozek R., Grin D., Marsh D. J. E., Ferreira P. G., 2015, Phys. Rev. D, 91, 103512

Hoffman G. L., Salpeter E. E., Farhat B., Roos T., Williams H., Helou G., 1996, ApJS, 105, 269

Horiuchi S., Bozek B., Abazajian K. N., Boylan-Kolchin M., Bullock J. S., Garrison-Kimmel S., Onorbe J., 2016, MNRAS, 456, 4346

Hu W., Barkana R., Gruzinov A., 2000, Phys. Rev. Lett., 85, 1158

Hui L., Ostriker J. P., Tremaine S., Witten E., 2017, Phys. Rev. D, 95, 043541 Kam Z. S., Carignan C., Chemin L., Amram P., Epinat B., 2015, MNRAS,

Kam Z. S., Carignan C., Chemin L., Amram P., Epinat B., 2015, MNRAS 449, 4048

Kaplinghat M., Tulin S., Yu H.-B., 2016, Phys. Rev. Lett., 116, 041302 Karukes E. V., Salucci P., Gentile G., 2015, A&A, 578, A13

Kirby E. N., Bullock J. S., Boylan-Kolchin M., Kaplinghat M., Cohen J. G., 2014, MNRAS, 439, 1015

Klypin A., Kravtsov A. V., Valenzuela O., Prada F., 1999, ApJ, 522, 82 Kuzio de Naray R., McGaugh S. S., de Blok W. J. G., 2008, ApJ, 676, 920

Lee, T.D.and Pang Y., 1989, Nucl. Phys. B, 315, 477

Lee J.-W., Koh I.-G., 1996, Phys. Rev. D, 53, 2236

Lelli F., McGaugh S. S., Schombert J. M., 2016, AJ, 152, 157

Li B., Rindler-Daller T., Shapiro P. R., 2014, Phys. Rev. D, 89, 083536

Lin S.-C., Schive H.-Y., Wong S.-K., Chiueh T., 2018, Phys. Rev. D, 97, 103523

Lora V., 2015, ApJ, 807, 116

Lora V., Magaña J., 2014, J. Cosmol. Astropart. Phys., 2014, 011

Lora V., Magaña J., Bernal A., Sánchez-Salcedo F. J., Grebel E., 2012, J. Cosmol. Astropart. Phys., 2012, 011

Lundgren A. P., Bondarescu M., Bondarescu R., Balakrishna J., 2010, ApJ, 715, L35

Macciò A. V., Dutton A. A., Van Den Bosch F. C., 2008, MNRAS, 391, 1940 Marsh D. J. E., Silk J., 2014, MNRAS, 437, 2652

Martinez-Medina L. A., Robles V. H., Matos T., 2015, Phys. Rev. D, 91, 023519

Matos T., Ureña-López L. A., 2004, Int. J. Mod. Phys. D, 13, 2287

Matos T., Guzmán F., Ureña-López L. A., 2000, Class. Quantum Gravity, 17, 1707

Matos T., Vázquez-González A., Magaña J., 2009, MNRAS, 393, 1359

McGaugh S. S., Schombert J. M., 2014, AJ, 148, 77

McGaugh S. S., Schombert J. M., 2015, ApJ, 802, 18

McGaugh S. S., Rubin V. C., de Blok W. J. G., 2001, AJ, 122, 2381

Meidt S. E. et al., 2014, ApJ, 788, 144

Mocz P., Vogelsberger M., Robles V. H., Zavala J., Boylan-Kolchin M., Fialkov A., Hernquist L., 2017, MNRAS, 471, 4559

Moore B., 1994, Nature, 370, 629

Moore B., Ghigna S., Governato F., Lake G., Quinn T., Stadel J., Tozzi P., 1999, ApJ, 524, L19

Navarro J. F., Eke V. R., Frenk C. S., 1996, MNRAS, 283, L72

Navarro J. F., Frenk C. S., White S. D. M., 1997, ApJ, 490, 493

Oman K. A. et al., 2015, MNRAS, 452, 3650

Oñorbe J., Boylan-Kolchin M., Bullock J. S., Hopkins P. F., Kereš D., Faucher-Giguère C.-A., Quataert E., Murray N., 2015, MNRAS, 454, 2092

Papastergis E., Shankar F., 2016, A&A, 591, A58

Papastergis E., Giovanelli R., Haynes M. P., Shankar F., 2015, A&A, 574, A113

Peñarrubia J., Pontzen A., Walker M. G., Koposov S. E., 2012, ApJ, 759, L42

Pizzella A., Corsini E. M., Sarzi M., Magorrian J., Méndez-Abreu J., Coccato L., Morelli L., Bertola F., 2008, MNRAS, 387, 1099

Planck Collaboration XXIII, 2015, A&A, 594, A13

Read J. I., Agertz O., Collins M. L. M., 2016, MNRAS, 459, 2573

Robles V. H. et al., 2017, MNRAS, 472, 2945

Robles V. H., Matos T., 2012, MNRAS, 422, 282

Robles V. H., Matos T., 2013, ApJ, 763, 19

Robles V. H., Lora V., Matos T., Sánchez-Salcedo F. J., 2015, ApJ, 810, 99

Rocha M., Peter A. H. G., Bullock J. S., Kaplinghat M., Garrison-Kimmel S., Oñorbe J., Moustakas L. A., 2013, MNRAS, 430, 81

Sarkar A., Mondal R., Das S., Sethi S., Bharadwaj S., Marsh D. J., 2016, J. Cosmol. Astropart. Phys., 2016, 012

Schive H.-Y., Liao M.-H., Woo T.-P., Wong S.-K., Chiueh T., Broadhurst T., Hwang W.-Y. P., 2014, Phys. Rev. Lett., 113, 261302

Schive H.-Y., Chiueh T., Broadhurst T., 2014, Nature Phys., 10, 496

Schive H.-Y., Chiueh T., Broadhurst T., Huang K.-W., 2016, ApJ, 818, 89

Schneider A., Smith R. E., Macciò A. V., Moore B., 2012, MNRAS, 424, 684

Schwabe B., Niemeyer J. C., Engels J. F., 2016, Phys. Rev. D, 94, 043513

Seidel E., Suen W.-M., 1990, Phys. Rev. D, 42, 384

Seidel E., Suen W.-M., 1994, Phys. Rev. Lett., 72, 2516

Sikivie P., Yang Q., 2009, Phys. Rev. Lett., 103, 111301

Simon J. D., Geha M., 2007, ApJ, 670, 313

Simon J. D., Bolatto A. D., Leroy A., Blitz L., Gates E. L., 2005, ApJ, 621, 757

Spergel D. N., Steinhardt P. J., 2000, Phys. Rev. Lett., 84, 3760

Suárez A., Chavanis P.-H., 2017, Phys. Rev. D, 95, 063515

Suárez A., Matos T., 2011, MNRAS, 416, 87

Tollerud E. J., Boylan-Kolchin M., Bullock J. S., 2014, MNRAS, 440, 3511 Tollet E. et al., 2016, MNRAS, 456, 3542

Ureña López L., 2002, Class. Quantum Gravity, 19, 2617

Ureña López L. A., Robles V. H., Matos T., 2017, Phys. Rev. D, 96, 043005

Veltmaat J., Niemeyer J. C., 2016, Phys. Rev. D, 94, 123523

Vogelsberger M. et al., 2014, MNRAS, 444, 1518

Vogelsberger M., Zavala J., Loeb A., 2012, MNRAS, 423, 3740

Vogelsberger M., Zavala J., Cyr-Racine F.-Y., Pfrommer C., Bringmann T., Sigurdson K., 2016, MNRAS, 460, 1399

Zavala J., Vogelsberger M., Walker M. G., 2013, MNRAS, 431, L20 Zolotov A. et al., 2012, ApJ, 761, 71

This paper has been typeset from a TeX/LATeX file prepared by the author.